Prediction of Response to ^{177}Lu-PSMA Therapy Based on Tumor-to-Kidney Ratio on Pretherapeutic PSMA PET/CT and Posttherapeutic Tumor-Dose Evaluation in mCRPC

Melanie Hohberg, Manuel Reifegerst, Alexander Drzezga, Markus Wild, and Matthias Schmidt

Department of Nuclear Medicine and Cancer Center Cologne, University Hospital of Cologne, Cologne, Germany

The aim of this study was to analyze the absorbed dose of ^{177}Lu-PSMA in osseous versus lymphatic metastases in patients with metastatic castration-resistant prostate cancer across therapy cycles and to relate those data to therapeutic success. In addition, pretherapeutic prostate-specific membrane antigen (PSMA) PET/CT was evaluated for its ability to predict response behavior. **Methods:** The study comprised 30 patients with metastatic castration-resistant prostate cancer, each receiving at least 3 cycles of ^{177}Lu-PSMA therapy. Prostate-specific antigen (PSA) values between baseline and 6 wk after the third therapy cycle were used to classify the patients as responders (PSA decline $\geq$ 50%) or nonresponders (unchanged or increasing PSA level). Quantitative SPECT/CT images were acquired 24, 48, and 168 h after application of ^{177}Lu-PSMA. The absorbed dose for tumor lesions was calculated with dosimetry software. From the pretherapeutic PET/CT scan, the tumor-to-kidney uptake ratio was determined for different SUVs. **Results:** Regardless of patient response, the kidneys received a mean dose of 0.55 $\pm$ 0.20 Gy/GBq per cycle. In the first therapy cycle, the lymph node lesions received a mean dose of 3.73 $\pm$ 1.65 Gy/GBq in responders and 1.86 $\pm$ 1.25 Gy/GBq in nonresponders ($P < 0.01$). For bone lesions, the respective mean doses were 3.47 $\pm$ 2.00 Gy/GBq and 1.48 $\pm$ 0.95 Gy/GBq ($P < 0.01$). When successive therapy cycles were compared, the mean dose was found to have been reduced from the first to the second cycle by 27% for lymph nodes and by 33% for bone lesions. A significant difference ($P < 0.01$) in the ratio of lymph node and bone lesion uptake to kidney uptake between responders and nonresponders could be deduced from the pretherapeutic PET/CT scan. **Conclusion:** Significantly higher doses were achieved for lymph node and bone lesions in responders. The highest absorbed dose, for both lymphatic and osseous lesions, was achieved in the first cycle, decreasing in the second therapy cycle thereafter despite unchanged therapy activities. It may be possible to estimate the response to therapy from the ratio of tumor uptake to kidney uptake obtained from the pretherapeutic PSMA PET/CT scans.

Key Words: PSMA therapy; prediction of therapy response; dosimetry; prostate cancer

Peptide radioligand therapy with prostate-specific membrane antigen (PSMA) ligands is now accepted for the treatment of metastases of advanced, castration-resistant prostate cancer for which both hormonal therapy and chemotherapy are no longer effective (1,2). To date, the treatment has been found to deliver good results with low side effects. Various clinical studies have shown that tumor growth can be slowed or tumor size greatly reduced with the help of radioligand therapy (3–9). The therapy is able to reduce the tumor load, thus lowering the prostate-specific antigen (PSA) level, and also to reduce pain, thereby significantly improving the patient's quality of life. However, experience has shown that although some patients respond well to ^{177}Lu-PSMA therapy, others respond poorly. The key may lie in individual differences in the degree to which the tracer accumulates in tumor lesions and hence differences in the absorbed tumor dose. A possible correlation between tumor dose and therapy outcome has already been explored in several papers (10–12). However, different methodologic approaches were taken. For example, some studies distinguished between responders and nonresponders but not between the different types of metastatic lesions, that is, lymph node or osseous involvement. In other studies, a distinction was made between lymph node and osseous metastases, but the patient group was not divided into responders and nonresponders. The aim of this work was to combine both approaches. The patients were divided into responders and nonresponders according to their response to therapy, as reflected in PSA decline, and at the same time differences between lymph node and bone lesions were evaluated. The correlation of tumor dose and therapy outcome is of course important, but even more valuable would be to predict the likelihood of response before radioligand therapy by means of a marker. This study investigated whether pretherapeutic PSMA PET/CT imaging could be used to predict therapy response (and hence the course of therapy).

MATERIALS AND METHODS

Study Population

Between March 2020 and February 2022, 30 patients with metastatic castration-resistant prostate cancer were enrolled in our study and underwent at least 3 cycles of ^{177}Lu-PSMA therapy (^{177}Lu-PSMA-I&T).

All patients had undergone radical prostatectomy before ^{177}Lu-PSMA therapy. Patients with a good treatment response received up to 6 cycles. Sufficient PSMA avidity for therapy was defined on ^{18}F-PSMA-7 or ^{68}Ga-PSMA PET/CT before the therapy. To minimize renal toxicity due to impaired renal function or excretory problems, ^{99m}Tc-mercaptoacetyltriglycine scintigraphy was performed before every therapy cycle.

This study was conducted in accordance with the requirements of the Institutional Review Board. All patients gave written informed consent to receive PSMA PET/CT and radioligand therapy and imaging and to have their data included in a retrospective analysis. All procedures were performed in compliance with the regulations of the responsible local authorities (District Administration of Cologne, Germany).

Radiotracer

Pretherapeutic Imaging. Pretherapeutic PET imaging was performed using ^{18}F-PSMA-7 (^{18}F-JK-PSMA-7) or ^{68}Ga-PSMA (^{68}Ga-PSMA-HBED-CC). The preparations of both tracers have been described previously (*13,14*). ^{18}F-PSMA-7 or ^{68}Ga-PSMA was administered to patients on a weight-adjusted basis of 5.0 MBq/kg and 2.5 MBq/kg, respectively.

Therapy. High-purity lutetium chloride (^{177}LuCl$_3$) was obtained from ITG, and PSMA-I&T was purchased from ABX. ^{177}Lu-PSMA-I&T was synthesized and labeled according to a previously published protocol (*15*). Patients received a mean activity of 7,209 ± 379 MBq of ^{177}Lu-PSMA-I&T for each therapy cycle.

Acquisition and Image Reconstruction

All PET/CT scans were obtained on a Biograph mCT device (mCT 128 Flow Edge; Siemens). Imaging started with a low-dose nonenhanced CT scan (120 kV, tube current modulation, pitch of 1.2, slice thickness of 5.0 mm) for attenuation correction followed by a whole-body PET scan from the base of the skull to the mid thigh. Reconstruction was conducted with an ordered-subset expectation maximization algorithm with 4 iterations and 12 subsets and gaussian-filtered to a transaxial resolution of 5 mm in full width at half maximum.

Quantitative SPECT/CT images (xSPECT; Siemens) were acquired at 24, 48, and 168 h after application of ^{177}Lu-PSMA-I&T on a Symbia Intevo Bold system (Siemens). The same time points were chosen for each therapy cycle. If no lesions in the head region were of interest for dosimetry, images of the thorax and abdomen were acquired at 2 bed positions. For attenuation correction, a low-dose CT scan (110 kV, 30 mAs, pitch of 1.5, slice thickness of 3.0 mm) was acquired alongside each SPECT scan. The SPECT images were reconstructed with an ordered-subset conjugate gradient maximization algorithm. For quantitative imaging, the device was regularly calibrated for ^{177}Lu according to the manufacturer's protocol.

Image Evaluation

Radiation dosimetry was performed using dosimetry software (MIM SurePlan MRT; MIM Software). Lesions were contoured on the first SPECT scan of each cycle using a gradient-based segmentation algorithm (PET Edge+; MIM Software). Once the user clicks anywhere within the region of interest, the algorithm begins to move outward, like a balloon slowly expanding. As the balloon expands, the algorithm is checking the gradient of the proposed contour until it reaches the optimal condition. The accuracy of the PET Edge+ tool has already been verified for PET imaging in other studies (*16,17*). A maximum of 5 lymph node lesions or 5 bone lesions per patient that were visually suggestive of prostate cancer metastases were counted and analyzed. Lesions with a volume smaller than 10 cm^3 were not considered. In addition to the lesions, the kidneys were automatically segmented on the first CT image, using an artificial intelligence algorithm (Contour Protégé AI; MIM Software). Lesions and the kidneys were resegmented for each therapy cycle in the same way. All SPECT and CT datasets were automatically coregistered by multiple local rigid registrations for each region of interest. The spatially aligned images are then used to calculate time–activity curves and the absorbed doses. The MIM Software provides a voxel-by-voxel curve fitting and integration. Curves are fitted by minimizing the squared differences between the curve from the selected function and the observed data points. The curve-fitting options are trapezoid plus exponential, monoexponential, biexponential, biexponential (fixed second λ), biexponential (forced zero at uptake time 0), and automatically determined, which finds the best fitting model from the monoexponential and biexponential options. The metric used to evaluate each equation is the Akaike information criterion, which evaluates the loss of information when a model is used to approximate the true distribution. The lowest Akaike information criterion value corresponds to the lowest information loss, and the model with the lowest Akaike information criterion is chosen on a voxel-by-voxel basis. The automatically determined curve fitting was selected in each case. The calculation of absorbed dose is based on the voxel S-value convolution method according to MIRD pamphlet 17. The voxel S-value convolution kernel was derived from Monte Carlo simulations with MCNP 6.2.2. The voxel S-value convolution kernels are simulated assuming the density of water for the MIRD 17 kernels. Therefore, a correction is necessary for tissues with heterogeneous densities. The absorbed dose map was corrected for physical density by applying a physical density map derived from the CT scan, with Hounsfield units being mapped to physical density values using a bilinear fit curve. The Hounsfield units are derived by scanning a CT density phantom using the same CT protocol as will be used for the SPECT/CT image acquisition. The resulting dose maps are divided by the physical density map, providing a density-corrected absorbed dose calculation.

Time–activity curve and dose volume histograms were calculated for all segmented structures on a voxel-based level. The same lesions and the kidneys were segmented on the corresponding pretherapeutic PET/CT scans. From these segmented structures, the mean ratio of lesion uptake to kidney uptake was calculated for SUV$_{max}$, SUV$_{peak}$, SUV$_{mean}$, and SUV$_{median}$.

An in-house workflow was created to calculate the total tumor burden (TTB) and the distribution to lymph nodes and bone lesions for each patient. In this workflow, a bone mask containing the entire bone volume of the patient is generated on the CT scan. Using the PET Edge+ tool, all lesions larger than 10 cm^3 are segmented. The bone mask is used to separate the bone lesions from the lymph nodes. At the same time, all segmented standard organs are also separated from the TTB.

For all segmented lesions, partial-volume correction was based on 2 phantom measurements with the National Electrical Manufacturers Association–International Electrotechnical Commission PET body phantom. During the first measurement, all 6 spheres (diameters of 10, 13, 17, 22, 28, and 37 mm) were filled with an activity concentration of 1.35 MBq of ^{177}Lu-PSMA per milliliter at a sphere-to-background ratio of 10:1. In a second measurement, the same activity concentration and sphere-to-background ratio were used for a 60-mm-diameter sphere. These measurements also served to evaluate the PET Edge+ tool for SPECT imaging. Calculation of recovery coefficients was based on the segmented and nominal activity in each sphere (*18*). The recovery curve was fitted to apply them to arbitrary volumes. Partial-volume correction was also applied for the kidneys.

The corresponding phantom measurements were also performed on the PET/CT scanner for ^{18}F and ^{68}Ga at an activity concentration of 20 kBq/mL.

Response Assessment

Biochemical response assessment was based on PSA levels according to previously described protocols (*19*). Response was defined as a PSA decline of at least 50% and nonresponse as an unchanged PSA level or an increasing level. Baseline for the PSA value was acquired on the day of therapy or the day before. The last PSA value considered was 6 wk after the third therapy or on the day of the fourth therapy if this had taken place.

TABLE 1
Patient Characteristics ($n = 30$)

Parameter	Age (y)	Weight (kg)	Initial PSA (μg/L)	Activity (MBq)		
				First cycle	Second cycle	Third cycle
Mean	72.4	81.4	315	7,209	7,191	7,128
SD	7.56	15.9	466	379	537	536
Range	56–87	60–169	7–2,480	6,463–8,009	6,107–8,263	6,014–7,805

Statistical Analysis

The software package SPSS Statistics 29 (IBM) was used for statistical analysis. The mean absorbed doses in lymph node and bone lesions were compared between responders and nonresponders using a Mann–Whitney U test. Furthermore, the ratio of lesion to kidney uptake was compared between responders and nonresponders. Differences in absorbed dose among the 3 cycles of therapy were examined using a Wilcoxon test matched-pair signed-rank test. The Kolmogorov–Smirnov test and the Shapiro–Wilk test were used to test for normality of the distributions. A P value of less than 0.05 was considered statistically significant. All data are expressed as the mean and related SD.

RESULTS

The patients had an average age of 72 y (range, 56–87 y) and an average weight of 81 kg (range, 60–169 kg). The initial PSA value ranged from 3 to 2,480 μg/L. The mean time between the pretherapeutic PSMA PET/CT and the first radioligand therapy cycle was 34 d (range, 5–90 d). Follow-up analysis revealed no evidence of kidney, liver, or bone marrow toxicity between any 2 cycles of therapy in any patient. Patient characteristics are summarized in Table 1. Detailed information on treatments before the first therapy, as well the TTB and distribution among lymph nodes and bone lesions, is presented in Supplemental Table 1 (supplemental materials are available at http://jnm.snmjournals.org). The change in PSA value with each cycle of therapy for each patient is listed in Supplemental Table 2.

Partial-Volume Correction

Results and details on the partial-volume correction and evaluation of the PET Edge+ tool for SPECT imaging can be found in
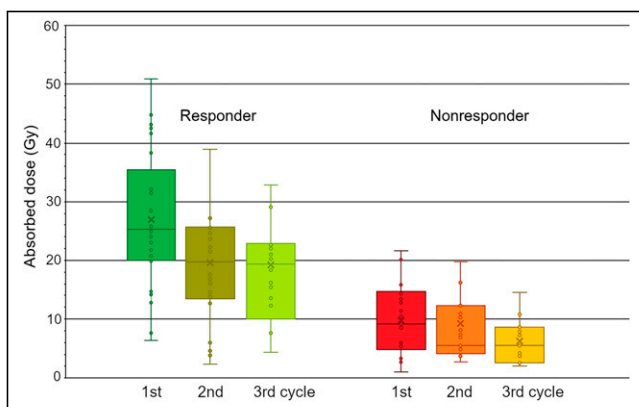
Supplemental Tables 3 and 4. Furthermore, the recovery coefficient curve can be found in Supplemental Figure 1.

Kidney Dosimetry

The mean absorbed kidney dose did not differ significantly ($Z = -0.73$; $P = 0.47$) between responders (0.53 ± 0.21 Gy/GBq) and nonresponders (0.56 ± 0.20 Gy/GBq), nor did it change significantly between the separate therapy cycles ($Z \geq -0.69$; $P \geq 0.44$). All results for the individual therapy cycles are presented in Table 2 and Supplemental Table 5.

Dosimetry for Lymph Node and Bone Lesions

In total, 77 suggestive lesions were analyzed, including 37 lymph node lesions and 40 bone lesions. The number of lesions was evenly distributed between responders and nonresponders. Individual tumor volumes used for analysis are summarized in Supplemental Table 6.

In the first therapy cycle, the responders received a mean dose of 3.73 ± 1.65 Gy/GBq for lymph node lesions and the nonresponders 1.86 ± 1.25 Gy/GBq. For the second therapy cycle, the mean absorbed dose for lymph nodes was reduced to 2.73 ± 1.48 Gy/GBq for responders and to 1.81 ± 1.45 Gy/GBq for nonresponders. In the third cycle, the dose dropped to 2.71 ± 1.55 Gy/GBq for responders and to 1.74 ± 1.55 Gy/GBq for nonresponders. The difference between the first and second therapy cycles and between responders and nonresponders was significant ($P < 0.01$).

A similar pattern was found for bone lesions in responders and nonresponders. In the first cycle, a mean dose of 3.47 ± 2.00 Gy/GBq was achieved for osseous metastases in responders, compared with a mean dose of 1.48 ± 0.95 Gy/GBq in nonresponders. In the second and third cycles, responders received mean doses of 2.32 ± 0.96 Gy/GBq and 1.73 ± 0.79 Gy/GBq, respectively, whereas nonresponders received 1.31 ± 0.91 Gy/GBq and 1.31 ± 0.94 Gy/GBq, respectively. The difference between the first and second therapy cycles and between responders and nonresponders was significant ($P < 0.01$).

FIGURE 1. Mean dose for lymph node lesions differentiated between responders and nonresponders over 3 therapy cycles.

TABLE 2
Results for Mean Kidney Dose Divided into Responder and Nonresponder

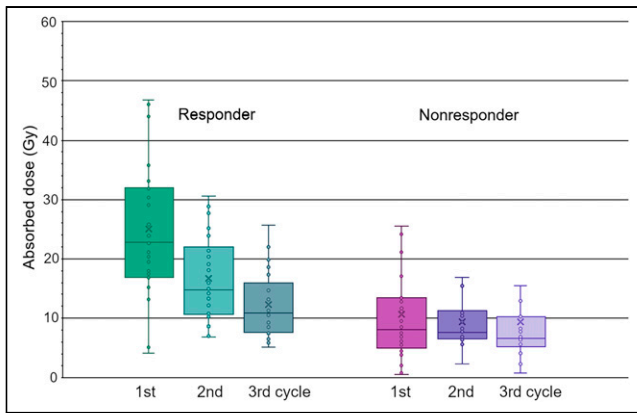| Parameter	Mean dose (Gy/GBq)		
	First cycle	Second cycle	Third cycle
Responder	0.53 ± 0.21	0.55 ± 0.22	0.56 ± 0.12
Nonresponder	0.56 ± 0.20	0.57 ± 0.18	0.55 ± 0.12
Z	−0.73	−0.68	−0.61
P	0.47	0.45	0.43

FIGURE 2. Mean dose for bone lesions differentiated between responders and nonresponders over 3 therapy cycles.

Over the course of the therapy cycles, the dose for responders decreased with each cycle, but only between the first and second cycles was the difference statistically significant ($P = 0.001$ for lymph nodes and $P = 0.003$ for bone lesions). There were no significant differences in absorbed dose between the second and third cycles for responders ($P = 0.126$ for lymph nodes and $P = 0.220$ for bone lesions). In nonresponders, the absorbed dose also decreased with each cycle of therapy, but none of the declines in dose was statistically significant ($P > 0.400$). Similar to the decrease in dose, the residence time also decreased with each subsequent therapy cycle. Again, significant differences were observed only between the first and second cycles ($P < 0.01$). Regardless of whether one considers lymph nodes or bone lesions in responders, the residence time halved from the first to the second therapy cycle. This halving of the residence time was not seen in nonresponders. However, the mean residence time in nonresponders was already 45% lower in lymph nodes and 54% lower in bone lesions in the first therapy cycle. An overview of the results is presented in Figures 1 and 2 and in Supplemental Tables 7–9.

In addition to the achieved dose, the TTB also changed over the course of therapy cycles. In patients who responded to therapy, the TTB decreased by $52.3\% \pm 4.7\%$ on average. In the group of nonresponders, the TTB decreased less or even increased again overall. With regard to only the tumor volume of the lesions considered for dosimetry, responders were found to have a mean decrease of 54.5% and nonresponders a mean decrease of 30.8%. Already-treated lesions appeared to diminish in nonresponders while new lesions appeared. The corresponding data are given in Supplemental Table 10.

Ratio of Tumor to Kidney Uptake in Pretherapeutic PET/CT Scan

This evaluation was based on a total of 19 scans with ^{18}F-PSMA-7 PET/CT and 11 with ^{68}Ga-PSMA PET/CT.

Kidney uptake measured as SUV_{max}, SUV_{peak}, SUV_{mean}, and SUV_{median} was equal in responders and nonresponders. On average, the SUVs for ^{68}Ga were 36% higher than those for ^{18}F, but this applied to the kidneys and lesions alike. Detailed information on the individual SUVs for ^{68}Ga and ^{18}F is shown in Supplemental Table 11.

The pretherapeutic PSMA PET/CT was acquired on average 1 mo (mean, 30.6 ± 10.4 d) before the first therapy cycle. There was a significant difference ($P < 0.01$) in the ratio of tumor-to-kidney uptake between responders and nonresponders. This difference applied to both lymph node and bone lesions. Uptake in lesions was about a factor of 2 higher than kidney uptake in responders ($P < 0.01$). The ratio of tumor uptake to kidney uptake correlated with the mean dose between responders and nonresponders. The mean dose was also 2 times higher for responders than for nonresponders. Again, this applied to lymph node and bone lesions in the same way. For the tumor-to-kidney uptake ratio, similar values were obtained, regardless of whether SUV_{peak}, SUV_{max}, SUV_{mean}, or SUV_{median} was used for the calculations. All results are summarized in Tables 3 and 4. Figures 3 and 4 show results from a responder and a nonresponder, respectively, including the tumor-to-kidney uptake ratio and the decrease or increase in TTB.

DISCUSSION

Three main findings emerged from the study: responders to ^{177}Lu-PSMA therapy achieved higher absorbed doses than nonresponders, absorbed doses decreased over the 3 therapy cycles, and tumor-to-kidney uptake ratio may serve as a parameter to identify potential responders on a pretherapeutic PSMA PET/CT scan.

The mean kidney dose did not differ significantly between responders and nonresponders, a total kidney dose of 0.55 ± 0.20 Gy/GBq being measured in both groups. The calculated mean dose for the kidneys was comparable to previously published data (10,20–22). A threshold dose for the human kidneys (20 Gy) would thus be exceeded only after more than 6 therapy cycles (23). Partial-volume correction for the kidneys was based on the largest sphere, which does not correspond to the anatomic shape of the kidneys. This represents a limitation of the kidney dose thus determined.

TABLE 3
Mean Dose for Lymph Node Lesions and Corresponding Lesion-to-Kidney Ratio

Parameter	Mean dose, first cycle (Gy/GBq)	Lesion-to-kidney ratio			
		SUV_{peak}	SUV_{mean}	SUV_{median}	SUV_{max}
Responder	3.73 ± 1.65	1.59 ± 0.73	1.57 ± 0.58	1.44 ± 0.57	1.58 ± 0.71
Nonresponder	1.86 ± 1.25	0.74 ± 0.47	0.85 ± 0.43	0.78 ± 0.39	0.80 ± 0.58
Ratio*	2.00	2.14	1.85	1.83	1.97
Z	-2.71	-4.75	-4.20	-4.75	-4.75
P	<0.01	<0.01	<0.01	<0.01	<0.01

*Responder to nonresponder.

TABLE 4
Mean Dose for Bone Lesions and Corresponding Lesion-to-Kidney Ratio

Parameter	Mean dose, first cycle (Gy/GBq)	Lesion-to-kidney ratio			
		SUV_{peak}	SUV_{mean}	SUV_{median}	SUV_{max}
Responder	3.47 ± 2.00	1.62 ± 0.79	1.59 ± 0.62	1.44 ± 0.61	1.61 ± 0.78
Nonresponder	1.48 ± 0.95	0.60 ± 0.35	0.79 ± 0.44	0.71 ± 0.39	0.78 ± 0.40
Ratio*	2.34	2.68	2.01	2.03	2.05
Z	-4.05	-5.18	-4.63	-5.10	-4.63
P	<0.01	<0.01	<0.01	<0.01	<0.01

*Responder to nonresponder.

Other studies reported similar mean tumor doses (*12*) and higher tumor doses (*11*) for ^{177}Lu-PSMA-617. A direct comparison of our findings with those obtained in previous studies is not feasible because of the differing procedures and software products used. Furthermore, the composition of the study groups varied: some authors distinguished responders from nonresponders (*10,11*), others characterized only lymph node or bone lesions (*12*), and in one study only the course of the mean dose over several cycles was analyzed (*24*).

Our results for lymph node and bone lesions contrast with previous findings (*12*) in which no difference in absorbed doses was evident between the first and second therapy cycles. However, the focus there was on very small lesions less than 1 cm^3. Furthermore, different activities were administered in the first (3 GBq) and second (6 GBq) therapy cycles, thus potentially compensating for a decrease in absorbed dose in subsequent cycles. Our data actually suggest the opposite, namely that patients might well benefit from a higher activity administered in the first cycle since the absorbed dose was found to decrease significantly from the first to the second cycle of therapy. A similar decrease in tumor dose over successive therapy cycles was observed by Okamoto et al. (*24*). Our data suggest that the observed decrease in absorbed dose may be related to a decrease in residence time. It remains unclear whether this decrease may be due to reduction or damage of PSMA receptors by the initial therapy. No further dose decrease could be observed between the second and third cycles. Rather, the dose achieved remained constant in both responders and nonresponders. Whether this also applies to subsequent therapy cycles will be investigated in a further study.

In our study, no distinction was made between unchanged PSA level and PSA increase. Defining an unchanged PSA value as the initial PSA value $\pm$ 10% deviation, we found that 50% of nonresponders belong to this group. This, too, may have influenced our measure of further disease progression.

Compared with other studies, only 3 measurement points were chosen for dosimetry. However, this number should be sufficiently accurate, as results with a root-mean-squared error below 10% have already been achieved in other studies with only one late measurement point (*25,26*).

The lesion-to-kidney ratio based on the pretherapeutic PSMA PET/CT scan revealed a significant difference between responders and nonresponders. This difference was also reflected in the tumor dose reached and the
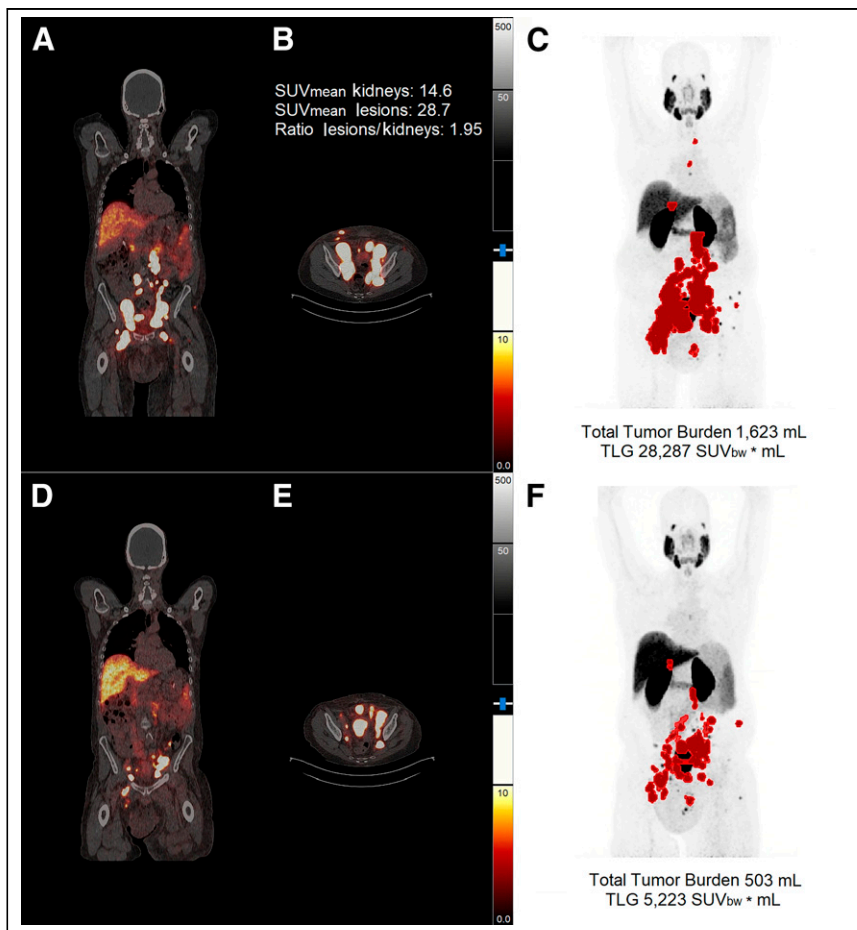

FIGURE 3. Results from one responder. (A–C) PET/CT imaging before first therapy cycle. (D–F) PET/CT imaging after 2 therapy cycles. (C and F) Maximum-intensity projections together with TTB and TLG. Lesions with SUV < 3.5 were not included. SUV_{bw} = standardized uptake value based on body weight.
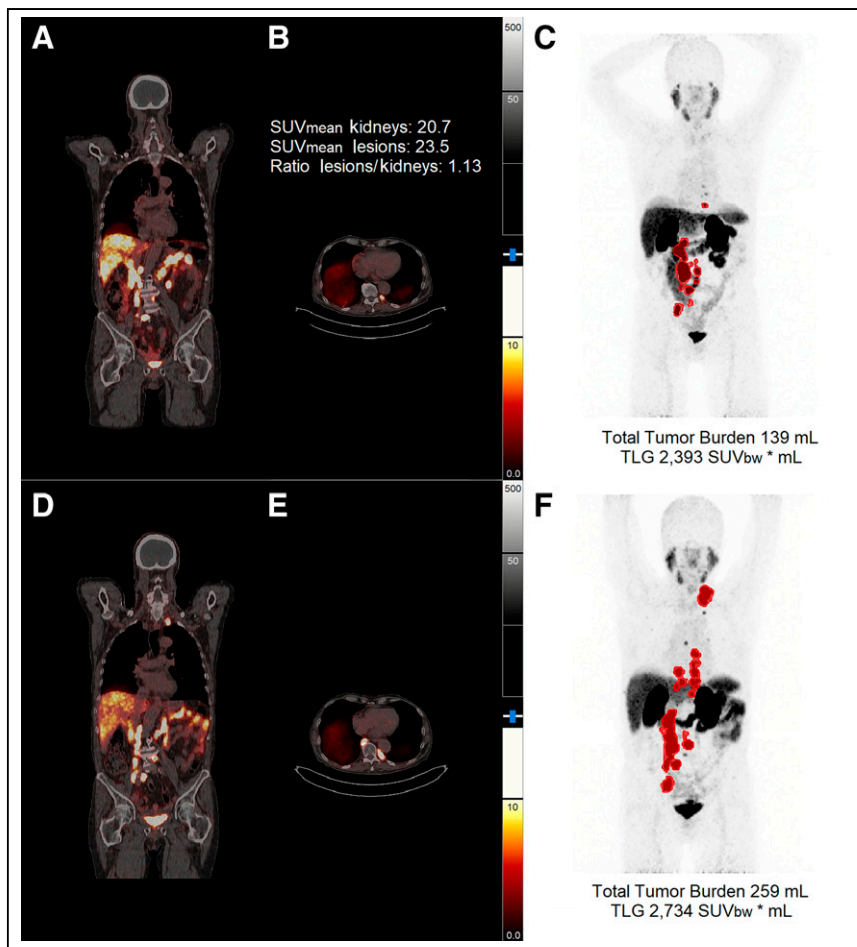
FIGURE 4. Results from one nonresponder. (A–C) PET/CT imaging before first therapy cycle. (D–F) PET/CT imaging after 2 therapy cycles. (C and F) Maximum-intensity projections together with TTB and TLG. Lesions with SUV < 3.5 were not included. SUV_{bw} = standardized uptake value based on body weight.

in tumor lesions was higher than 10 for responders and nonresponders.

So far, the response evaluation has been based on only biochemical response, with no long-term follow-up or survival data. Some patients reported here received up to 6 cycles. For now, the number of these patients is still too small for a valid statistical evaluation. However, even in this small group, a few tendencies are emerging for further treatment response, which will also be investigated together with overall survival in the future.

CONCLUSION

In lymph node and bone lesions, a significantly higher dose is absorbed in responders than nonresponders during the course of radioligand therapy with ^{177}Lu-PSMA-I&T. This difference is also reflected in the therapeutic success. The absorbed dose was highest in the first cycle and then decreased significantly in the second cycle. There is a case, therefore, for increasing the applied activity in the first cycle to maximize therapy success. The significant difference in the tumor-to-kidney uptake ratio between responders and nonresponders may serve as a predictor of treatment response. Further studies will be needed to examine this possibility.

DISCLOSURE

No potential conflict of interest relevant to this article was reported.

PSA decline. The ratio of tumor uptake to kidney uptake in pretherapeutic PET/CT may therefore serve as a predictor of treatment response. This information would be available even before the first therapy cycle, thereby allowing other therapy options to be considered. These might include therapy with [225]Ac-PSMA (27,28) at an early stage for patients who are likely to have a poor response to treatment with ^{177}Lu-PSMA ligands. PET/CT images with ^{18}F and ^{68}Ga were used to assess the lesion-to-kidney ratio. However, since no absolute SUVs but only relative ratios were compared between kidney and lesion uptake, this limitation should affect the results only minimally.

There are multiple studies suggesting the importance of pretherapeutic PET/CT in predicting response to ^{177}Lu-PSMA therapies (29,30). In contrast to the work of Khreish et al. (29), we cannot confirm that SUV_{peak} is less appropriate than SUV_{mean} as a predictor of therapy response. However, the tumor-to-liver uptake ratio was compared with progression-free survival in the study of Khreish et al. The tumor-to-liver ratio was not available in our patient collective because some patients also had metastases in the liver.

In the work by Buteau et al. (30), an SUV_{mean} of 10 or higher on PSMA PET was evaluated as a predictive biomarker for response to ^{177}Lu-PSMA-617. The cutoff proposed by Buteau et al. would not be transferable to our collective as the SUV_{mean}

KEY POINTS

QUESTION: Is there a clear difference between responders and nonresponders, and is it possible to predict the response to ^{177}Lu-PSMA therapy?

PERTINENT FINDINGS: In this study, 30 patients with metastatic castration-resistant prostate cancer undergoing ^{177}Lu-PSMA therapy were examined with regard to therapy response and the achieved dose for lymph nodes and bone metastases. A significant difference between responders and nonresponders was found. The response to therapy may be estimated from pretherapeutic PSMA PET/CT based on the lesion-to-kidney uptake ratio.

IMPLICATIONS FOR PATIENT CARE: An assessment of the therapy response allows other options to be considered or the applied activity to be adjusted.

REFERENCES

1. Sartor O, de Bono J, Chi KN, et al.; VISION Investigators. Lutetium-177–PSMA-617 for metastatic castration-resistant prostate cancer. *N Engl J Med.* 2021;385:1091–1103.
2. Schneider CA, Täger P, Hammes J, et al. Treatment outcome and identification of factors influencing overall survival after Lu-177-PSMA-617 radioligand therapy in metastatic castration-resistant prostate cancer. *Nuklearmedizin.* 2022;61:25–32.

3. Bander NH, Milowsky MI, Nanus DM, Kostakoglu L, Vallabhajosula S, Goldsmith SJ. Phase I trial of [177]lutetium-labeled J591, a monoclonal antibody to prostate-specific membrane antigen, in patients with androgen-independent prostate cancer. *J Clin Oncol.* 2005;23:4591–4601.

4. Tagawa ST, Milowsky MI, Morris M, et al. Phase II study of lutetium-177–labeled antiprostate-specific membrane antigen monoclonal antibody J591 for metastatic castration-resistant prostate cancer. *Clin Cancer Res.* 2013;19:5182–5191.

5. Kratochwil C, Giesel FL, Eder M, et al. (^{177}Lu)lutetium-labelled PSMA ligand-induced remission in a patient with metastatic prostate cancer. *Eur J Nucl Med Mol Imaging.* 2015;42:987–988.

6. Ahmadzadehfar H, Eppard E, Kurpig S, et al. Therapeutic response and side effects of repeated radioligand therapy with ^{177}Lu-PSMA-DKFZ-617 of castrate-resistant metastatic prostate cancer. *Oncotarget.* 2016;7:12477–12488.

7. Baum RP, Kulkarni HR, Schuchardt C, et al. Lutetium-177 PSMA radioligand therapy of metastatic castration-resistant prostate cancer: safety and efficacy. *J Nucl Med.* 2016;57:1006–1013.

8. Rahbar K, Ahmadzadehfar H, Kratochwil C, et al. German multicenter study investigating ^{177}Lu-PSMA-617 radioligand therapy in advanced prostate cancer patients. *J Nucl Med.* 2017;58:85–90.

9. Heck MM, Tauber R, Schwaiger S, et al. Treatment outcome, toxicity, and predictive factors for radioligand therapy with ^{177}Lu-PSMA-I&T in metastatic castration-resistant prostate cancer. *Eur Urol.* 2019;75:920–926.

10. Violet J, Jackson P, Ferdinandus J, et al. Dosimetry of ^{177}Lu-PSMA-617 in metastatic castration-resistant prostate cancer: correlations between pretherapeutic imaging and whole-body tumor dosimetry with treatment outcomes. *J Nucl Med.* 2019;60:517–523.

11. Völter F, Mittlmeier L, Gosewisch A, et al. Correlation of an index-lesion-based SPECT dosimetry method with mean tumor dose and clinical outcome after ^{177}Lu-PSMA-617 radioligand therapy. *Diagnostics (Basel).* 2021;11:428.

12. Peters SMB, Privé BM, de Bakker M, et al. Intra-therapeutic dosimetry of (^{177}Lu)Lu-PSMA-617 in low-volume hormone-sensitive metastatic prostate cancer patients and correlation with treatment outcome. *Eur J Nucl Med Mol Imaging.* 2022;49:460–469.

13. Hohberg M, Kobe C, Krapf P, et al. Biodistribution and radiation dosimetry of (^{18}F)-JK-PSMA-7 as a novel prostate-specific membrane antigen-specific ligand for PET/CT imaging of prostate cancer. *EJNMMI Res.* 2019;9:66.

14. Eder M, Schäfer M, Bauder-Wüst U, et al. ^{68}Ga-complex lipophilicity and the targeting property of a urea-based PSMA inhibitor for PET imaging. *Bioconjug Chem.* 2012;23:688–697.

15. Weineisen M, Simecek J, Schottelius M, Schwaiger M, Wester H-J. Synthesis and preclinical evaluation of DOTAGA-conjugated PSMA ligands for functional imaging and endoradiotherapy of prostate cancer. *EJNMMI Res.* 2014;4:63.

16. Werner-Wasik M, Nelson AD, Choi W, et al. What is the best way to contour lung tumors on PET scans? Multiobserver validation of a gradient-based method using a NSCLC digital PET phantom. *Int J Radiat Oncol Biol Phys.* 2012;82:1164–1171.

17. Obara P, Liu H, Wroblewski K, et al. Quantification of metabolic tumor activity and burden in patients with non-small-cell lung cancer: is manual adjustment of semiautomatic gradient-based measurements necessary? *Nucl Med Commun.* 2015;36:782–789.

18. Hoffman EJ, Huang SC, Phelps ME. Quantitation in positron emission computed tomography: 1. Effect of object size. *J Comput Assist Tomogr.* 1979;3:299–308.

19. Scher HI, Morris MJ, Stadler WM, et al. Trial design and objectives for castration-resistant prostate cancer: updated recommendations from the Prostate Cancer Clinical Trials Working Group 3. *J Clin Oncol.* 2016;34:1402–1418.

20. Hohberg M, Eschner W, Schmidt M, et al. Lacrimal glands may represent organs at risk for radionuclide therapy of prostate cancer with (^{177}Lu)DKFZ-PSMA-617. *Mol Imaging Biol.* 2016;18:437–445.

21. Delker A, Fendler WP, Kratochwil C, et al. Dosimetry for ^{177}Lu-DKFZ-PSMA-617: a new radiopharmaceutical for the treatment of metastatic prostate cancer. *Eur J Nucl Med Mol Imaging.* 2016;43:42–51.

22. Herrmann K, Rahbar K, Eiber M, et al. Dosimetry of ^{177}Lu-PSMA-617 for the treatment of metastatic castration-resistant prostate cancer: results from the VISION trial sub-study [abstract]. *J Clin Oncol.* 2022;40(suppl):97.

23. ICRP publication 118: ICRP statement on tissue reactions and early and late effects of radiation in normal tissues and organs—threshold doses for tissue reactions in a radiation protection context. *Ann ICRP.* 2012;41:1–322.

24. Okamoto S, Thieme A, Allmann J, et al. Radiation dosimetry for ^{177}Lu-PSMA I&T in metastatic castration-resistant prostate cancer: absorbed dose in normal organs and tumor lesions. *J Nucl Med.* 2017;58:445–450.

25. Rinscheid A, Kletting P, Eiber M, Beer AJ, Glatting G. Influence of sampling schedules on (^{177}Lu)Lu-PSMA dosimetry. *EJNMMI Phys.* 2020;17;7:41.

26. Kurth J, Heuschkel M, Tonn A, et al. Streamlined schemes for dosimetry of ^{177}Lu-labeled PSMA targeting radioligands in therapy of prostate cancer. *Cancers (Basel).* 2021;13:3884.

27. Kratochwil C, Bruchertseifer F, Giesel FL, et al. [225]Ac-PSMA-617 for PSMA-targeted α-radiation therapy of metastatic castration-resistant prostate cancer. *J Nucl Med.* 2016;57:1941–1944.

28. Tauber RL, Feuerecker B, Knorr K, et al. Safety and efficacy of Ac-225-PSMA-617 in metastatic castration resistant prostate cancer (mCRPC) after failure of Lu-177-PSMA [abstract]. *Ann Oncol.* 2019;30(suppl 5):V342.

29. Khreish F, Wiessner M, Rosar F, et al. Response assessment and prediction of progression-free survival by ^{68}Ga-PSMA-11 PET/CT based on tumor-to-liver ratio (TLR) in patients with mCRPC undergoing ^{177}Lu-PSMA-617 radioligand therapy. *Biomolecules.* 2021;11:1099.

30. Buteau JP, Martin AJ, Emmett L, et al.; TheraP Trial Investigators and the Australian and New Zealand Urogenital and Prostate Cancer Trials Group. PSMA and FDG-PET as predictive and prognostic biomarkers in patients given (^{177}Lu)Lu-PSMA-617 versus cabazitaxel for metastatic castration-resistant prostate cancer (TheraP): a biomarker analysis from a randomised, open-label, phase 2 trial. *Lancet Oncol.* 2022;23:1389–1397.